

Coherent spin pumping in a strongly coupled magnon-magnon hybrid system

Yi Li,^{1,2} Wei Cao,³ Vivek P. Amin,^{4,5} Zhizhi Zhang,^{2,6} Jonathan Gibbons,² Joseph Sklenar,⁷ John Pearson,² Paul M. Haney,⁵ Mark D. Stiles,⁵ William E. Bailey,^{3,*} Valentine Novosad,^{2,†} Axel Hoffmann,^{2,†} and Wei Zhang^{1,2,‡}

¹*Department of Physics, Oakland University, Rochester, MI 48309, USA*

²*Materials Science Division, Argonne National Laboratory, Argonne, IL 60439, USA*

³*Materials Science and Engineering, Department of Applied Physics and Applied Mathematics, Columbia University, New York, New York 10027, USA*

⁴*Maryland Nanocenter, University of Maryland, College Park, MD 20742, USA*

⁵*Center for Nanoscale Science and Technology, National Institute of Standards and Technology, Gaithersburg, Maryland 20899, USA*

⁶*School of Optical and Electronic Information, Huazhong University of Science and Technology, Wuhan 430074, China*

⁷*Department of Physics and Astronomy, Wayne State University, Detroit, MI 48202, USA*

(Dated: November 1, 2019)

We experimentally identify coherent spin pumping in the magnon-magnon hybrid modes of permalloy/yttrium iron garnet (Py/YIG) bilayers. Using broadband ferromagnetic resonance, an “avoided crossing” is observed between the uniform mode of Py and the spin wave mode of YIG due to the fieldlike interfacial exchange coupling. We also identify additional linewidth suppression and enhancement for the in-phase and out-of-phase hybrid modes, respectively, which can be interpreted as concerted dampinglike torque from spin pumping. Our analysis predicts inverse proportionality of both fieldlike and dampinglike torques to the square root of the Py thickness, which quantitatively agrees with experiments.

Coherent information processing has recently become an emerging topic for the post-CMOS electronics era [1, 2]. In spintronics, exchange-induced magnetic excitations, called spin waves, or magnons [3, 4], are good candidates because information can be encoded by both the amplitude and the phase of spin waves. For example, the interference of coherent spin waves can be engineered for spin wave logic operations [5–7]; the coherent interaction of spin-torque oscillators leads to mutual synchronization [8–13], which can be applied in artificial neural networks [14, 15]; and the coherent coupling between magnons and microwave cavities [16–22] opens up new opportunities for magnon-based quantum information science [23, 24].

Recently, strong coupling between two magnonic systems has been observed [25–27], which allows excitations of forbidden spin wave modes and high group velocity of propagating spin waves [28, 29]. The coupling is dominated by the exchange interaction at the interface of the magnetic bilayers, providing a new pathway to coherently transfer magnon excitations between two magnetic systems possessing distinctive properties: from conductor to insulator, from uniform to nonuniform mode and from high-damping to low-damping systems. However, the underlying physical mechanisms of the coupling are still not fully understood. First, what are the key parameters that dictate the coupling efficiency and enable one to reach the strong-coupling regime? Second, with the interfacial exchange coupling acting as a fieldlike torque, is there a dampinglike torque associated with spin pumping [30–33]? The second question is particularly important for optimizing the coherence of spin wave transfer in hybrid systems. Furthermore, any parasitic effect on the incoherent spin current from the conduction band is well-

removed [34–36] by using magnetic insulators such as yttrium iron garnet ($\text{Y}_3\text{Fe}_5\text{O}_{12}$, YIG) [29, 37, 38], which facilitates the study of spin pumping coherency.

In this work, we study YIG/permalloy ($\text{Ni}_{80}\text{Fe}_{20}$, Py) bilayers with varying Py thicknesses. By using a much thinner YIG film compared with previous work [25, 27], we define well-separated perpendicular standing spin wave (PSSW) modes in YIG and create an avoided crossing much larger than the linewidths, allowing us to study the linewidth evolution of the two individual hybrid modes. We find a pronounced suppression of the total linewidth for in-phase hybrid modes and a linewidth enhancement for out-of-phase hybrid modes. The linewidths can be understood from the Landau-Lifshitz-Gilbert (LLG) equation with interfacial exchange coupling and mutual spin pumping, which provide the fieldlike and dampinglike interlayer coupling torques, respectively. The analysis also explains the thickness dependence of the two coupling strengths and reconfirms the antiferromagnetic coupling between YIG and Py [25]. Our results provide important insights for improving the coupling strength and coherence in magnon-magnon hybrid systems and pave the way for coherent information processing with exchange coupled magnetic heterostructures.

The samples consist of YIG(100 nm)/Py(t_{Py}) bilayers where t_{Py} varies from 5 nm to 60 nm. YIG(100 nm) films were deposited by magnetron sputtering from a YIG target onto $\text{Gd}_3\text{Ga}_5\text{O}_{12}$ (111) substrates and annealed in air to reach low-damping characteristics [39]. Before the deposition of Py films on top of YIG, the YIG surfaces were ion milled in vacuum for one minute in order to enable good exchange coupling between Py and YIG [40].

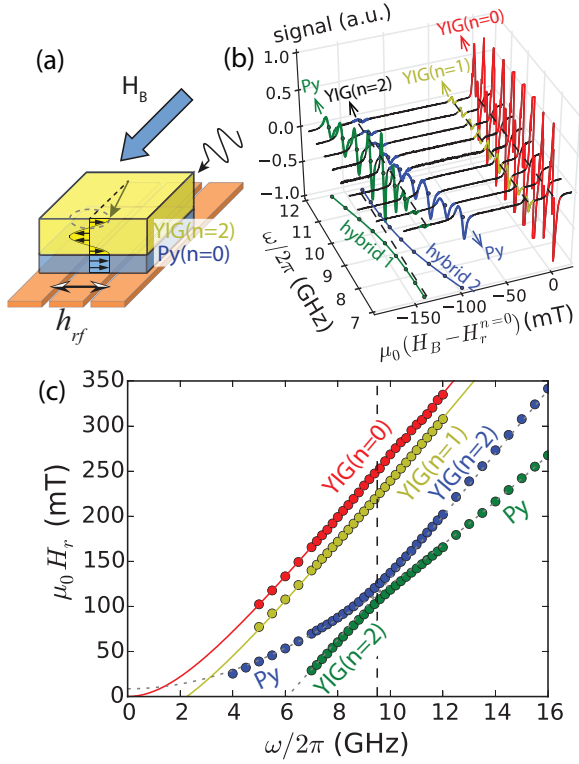


FIG. 1. (a) Illustration of the spin wave modes in the Py/YIG bilayers and the microwave excitation by a coplanar waveguide. (b) Lineshapes of the Py(9 nm)/YIG(100 nm) sample for the first three spin wave modes of YIG and the uniform mode of Py. The field axis is shifted that the resonance field of the YIG($n=0$) mode is zero. (c) Unshifted evolution of the four modes in (b). Curves show the fits of the four uncoupled modes. The vertical dashed line denotes where the YIG($n=2$) and Py($n=0$) modes cross on the frequency axis at $\omega_c/2\pi = 9.4$ GHz.

For each Py thickness, one additional, reference Py film was deposited on a Si/SiO₂ substrate during the same deposition.

The hybrid magnon dynamics were characterized by broad-band ferromagnetic resonance on a coplanar waveguide (Fig. 1a). An in-plane magnetic field H_B saturates both the YIG and Py magnetizations. Their Kittel modes, which describe spatially uniform magnetization precession, are formulated as $\omega^2/\gamma^2 = \mu_0^2 H_r (H_r + M_s)$, where ω is the mode frequency, $\gamma/2\pi = (g_{eff}/2) \times 27.99$ GHz/T is the gyromagnetic ratio, H_r is the resonance field and M_s is the magnetization. For the spatially nonuniform PSSW modes, specifically in YIG, an effective exchange field H_{ex} will lower the resonance field as $\mu_0 H_{ex}(k) = (2A_{ex}/M_s)k^2$, where A_{ex} is the exchange stiffness, $k = n\pi/t$, n labels the index of PSSW modes, and t is the film thickness.

Fig. 1(b) shows the line shapes of the resonance fields for the first three YIG PSSW modes ($n = 0, 1, 2$) and the Py uniform mode ($n = 0$) measured for $t_{Py} = 9$ nm.

For illustration, the YIG ($n = 0$) resonance is shifted to zero field. An avoided crossing is clearly observed when the Py uniform mode is degenerate with the YIG ($n = 2$) mode. This is due to the exchange coupling at the YIG/Py interface [25–27] providing a fieldlike torque. In addition, around degeneracy both two YIG-Py hybrid modes are strongly excited even when the YIG ($n = 2$) mode does not couple to the nearly uniform microwave field from the coplanar waveguide, because the energy of the Py uniform mode is coherently transferred to the YIG PSSW modes through the interface [25]. The full-range frequency dependence of the extracted resonance field are plotted in Fig. 1(c). To analyze the two hybrid modes, we analyze our results with two independent Lorentzians because it facilitates a transparent physical picture and the fit lineshapes agree well with our measurements. The modes crossing happens at $\omega_c/2\pi = 9.4$ GHz (black dashed line), which corresponds to the minimal resonance separation of the two hybrid modes. Fitting to the Kittel equation, we extract $\mu_0 M_s^{YIG} = 0.21$ T, $\mu_0 M_s^{Py} = 0.86$ T. From the exchange field offset as shown in Fig. 1(b), an exchange stiffness $A_{ex} = 2.6$ pJ/m is calculated for YIG, which is similar to previous reports [41].

The avoided crossing can be fitted to a phenomenological model of two coupled harmonic oscillators, as previously shown in magnon polaritons [16–18, 20]:

$$\mu_0 H_c^\pm = \mu_0 \frac{H_r^{YIG} + H_r^{Py}}{2} \pm \sqrt{\left(\mu_0 \frac{H_r^{YIG} - H_r^{Py}}{2} \right)^2 + g_c^2} \quad (1)$$

where $H_r^{YIG(Py)}$ is the resonance field of YIG (Py), and g_c is the interfacial exchange coupling strength. H_r^{YIG} and H_r^{Py} are both functions of frequency and are equal at ω_c . Note that for in-plane biasing field the resonance field is nonlinear to the excitation frequency. This nonlinearity will be accounted in the analytical reproduction of Eq. 1. The fitting yields $g_c = 8.4$ mT for $t_{Py} = 9$ nm.

Next, we focus on the linewidths of the YIG-Py hybrid modes, which reflect the existence of the damping-like torque in addition to the fieldlike torque from the interfacial exchange. Fig. 2(a) shows the line shape of the two hybrid modes for $t_{Py} = 7.5$ nm at ω_c . These two eigenmodes correspond to the in-phase and out-of-phase magnetization precession of Py and YIG with the same weight, so they should yield the same total intrinsic damping. Nevertheless, a significant linewidth difference is observed, with the extracted full-width-half-maximum linewidth $\mu_0 \Delta H_{1/2}$ varying from 3.5 mT for the lower field resonance to 8.0 mT for the higher field resonance. Fig. 2(b) shows the full-range evolution of linewidth. Compared with the dotted lines which are the linear extrapolations of the YIG ($n = 2$) and Py linewidths, the linewidth of the higher-field hybrid mode (blue circles) exceeds the Py linewidth and the linewidth

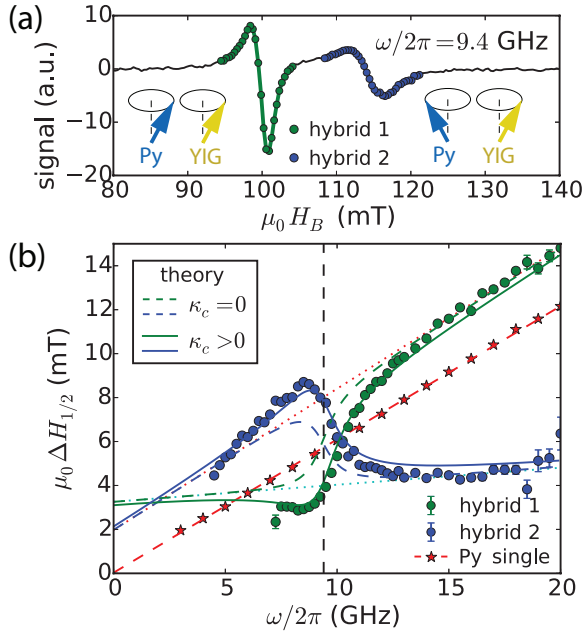


FIG. 2. (a) The lineshape of the Py(7.5 nm)/YIG(100 nm) sample at $\omega/2\pi = 9.4$ GHz, showing different linewidths between the two hybrid modes of YIG($n = 2$) and Py($n = 0$) resonances. (b) Linewidths of the two hybrid modes as a function of frequency. Dotted lines show the linear fit of the linewidths for the two uncoupled modes. Dashed curves show the theoretical values with $\kappa_{sp} = 0$. Solid curves show the fits with finite κ_{sp} .

of the lower-field hybrid mode (green circles) reduces below the YIG linewidth when the frequency is near ω_c . This is the central result of the paper. It suggests an additional dampinglike torque which acts along or against the intrinsic damping torque depending on the mode profile of the YIG/Py hybrid dynamics, same as the fieldlike exchange torque acting along or against the Larmor precession torque.

To reproduce the data in Fig. 2(b), we introduce the linewidths as the imaginary parts of the resonance fields in Eq. (1):

$$\mu_0(H_c^\pm + i\Delta H_{1/2}^\pm) = \mu_0 \frac{H_r^{\text{YIG}} + H_r^{\text{Py}}}{2} + i\mu_0 \frac{\kappa_{\text{YIG}} + \kappa_{\text{Py}}}{2} \pm \sqrt{\left(\mu_0 \frac{H_r^{\text{YIG}} - H_r^{\text{Py}}}{2} + i\mu_0 \frac{\kappa_{\text{YIG}} - \kappa_{\text{Py}}}{2} \right)^2 + \tilde{g}_c^2} \quad (2)$$

where $\kappa_{\text{YIG(Py)}}$ is the uncoupled linewidth of YIG (Py) from the linear extraction (dotted lines) in Fig. 2(b), and $\tilde{g}_c = g_c + i\kappa_c$ is the complex interfacial coupling strength with an additional dampinglike component κ_c . The dominate mechanism for κ_c is the mutual spin pumping from the concerted dynamics of YIG and Py [30, 31]. To compare with the uncoupled spin pumping, we quantify the latter as the linewidth enhancement of Py(7.5 nm), $\Delta H_{sp}^{\text{Py}}$, between the YIG/Py (red dots in Fig. 2b)

and Si/SiO₂/Py (red stars in Fig. 2b). Then we fit the experimental data by using $\kappa_c(\omega) = \beta\mu_0\Delta H_{sp}^{\text{Py}}(\omega)$. Here β is a unitless weight of the uncoupled spin pumping contribution to the dampinglike coupling, which will be discussed later. For the best fit value, $\beta = 0.82$, Eq. (2) nicely reproduce the data in Fig. 2. For comparison, if we set $\kappa_c = 0$ in Eq. (2), we obtain the blue and green dashed curves, which result in identical linewidth at ω_c as opposed to the data in Fig. 2(a).

In order to understand the physical meaning of \tilde{g}_c , we consider the coupled Landau-Lifshitz-Gilbert (LLG) equations of YIG/Py bilayer [25, 31, 33] in the macrospin limit:

$$\frac{d\mathbf{m}_i}{dt} = -\mu_0\gamma_i\mathbf{m}_i \times \mathbf{H}_{eff} + \alpha_i\mathbf{m}_i \times \frac{d\mathbf{m}_i}{dt} - \gamma_i\mathbf{m}_i \times \frac{J}{M_i t_i} \mathbf{m}_j + \Delta\alpha_i(\mathbf{m}_i \times \frac{d\mathbf{m}_i}{dt} - \mathbf{m}_j \times \frac{d\mathbf{m}_j}{dt}) \quad (3)$$

where $\mathbf{m}_{i,j}$ is the unit magnetization vector, \mathbf{H}_{eff} is the effective field including H_B , H_{ex} and the demagnetization field, α_i is the intrinsic Gilbert damping. The index is defined as $(i, j) = (1, 2)$ or $(2, 1)$. In the last two coupling terms, J is the interfacial exchange energy and $\Delta\alpha_i = \gamma_i\hbar g^{\uparrow\downarrow}/(4\pi M_i t_i)$ is the spin pumping damping enhancement. The two terms provide the fieldlike and dampinglike coupling torques, respectively, between \mathbf{m}_i and \mathbf{m}_j . To view the dampinglike coupling on a similar footage, we define its coupling energy J' as:

$$J'(\omega) = \frac{g^{\uparrow\downarrow}}{4\pi} \hbar\omega \quad (4)$$

Here J' describes the number of quantum channels per unit area ($g^{\uparrow\downarrow}$) for magnons ($\hbar\omega$) to pass through [30, 33]; similarly, J describes the number and strength of exchange bonds between YIG and Py per unit area. From the definition, we can express the spin pumping linewidth enhancement as $\mu_0\Delta H_{sp}^i = J'/M_i t_i$, in pair with the exchange field term in Eq. (3). By solving Eq. (3) we find:

$$\kappa_i = \frac{\alpha_i\omega}{\gamma_i} + \frac{J'}{M_i t_i} \quad (5a)$$

$$g_c = f(\omega_c) \cdot \sqrt{\frac{J}{M_1 t_1} \cdot \frac{J}{M_2 t_2}} \quad (5b)$$

$$\kappa_c = f(\omega_c) \cdot \sqrt{\frac{J'}{M_1 t_1} \cdot \frac{J'}{M_2 t_2}} \quad (5c)$$

with the dimensionless factor $f(\omega)$ accounting for the precession elliptical asymmetry. $f(\omega) = 1$ for identical ellipticity ($M_1 = M_2$) and $f(\omega_c) = 0.9$ in the case of YIG and Py; See the Supplemental Information for details [42]. Eq. (5) shows that both g_c and κ_c are proportional to $1/\sqrt{t_i}$, which comes from the geometric averaging of the coupled magnetization dynamics. This is in contrast to the $1/t_i$ dependence of the uncoupled exchange field and spin pumping damping enhancement for a single layer,

as shown in Eq. (5a). In Fig. 3(a), a good fitting of g_c to $1/\sqrt{t_{Py}}$ rather than t_{Py} validates the model. In the limit of zero Py thickness, the model breaks down due to the significance of boundary pinning and the assumption of macrospin dynamics. For the dampinglike coupling, because it is inconvenient to directly obtain the value of κ_c , we use the fit parameter β to represent it. By taking the spin pumping linewidth enhancement as $\mu_0\Delta H_{sp}^{Py} = J'/M_{Py}t_{Py}$, we obtain the macrospin expression $\beta = f(\omega_c)\sqrt{M_{Py}t_{Py}/M_{YIG}t_{YIG}}$. In Fig. 3(b) we plot the extracted β^2 for different t_{Py} , which follows a linear fit shown in a blue solid line.

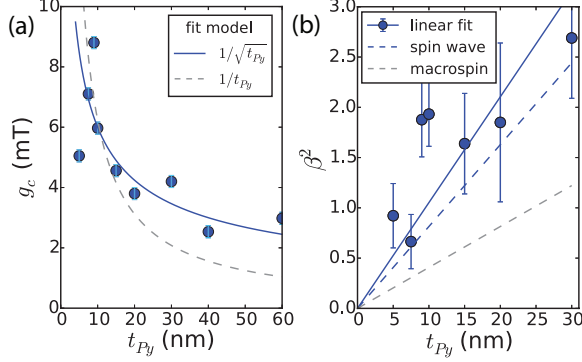


FIG. 3. (a) Extracted g_c as a function of t_{Py} . The solid and dashed curves show the fits to the dependence of $1/\sqrt{t_{Py}}$ and $1/t_{Py}$, respectively. (b) Extracted β^2 as a function of t_{Py} . The solid and dashed lines show the theoretical predictions of the spin wave model and macrospin model, respectively, which differ in slope by a factor of two. Error bars indicate single standard deviations found from the fits to the lineshape.

If we calculate β from measured values of M_i and t_{YIG} , we obtain a theoretical curve which differs significantly from the experimental data (gray dashed line in Fig. 3b). To account for the difference, we consider a spin wave model for the YIG/Py bilayer, where finite wavenumbers exist in both layers and are determined from the boundary condition [43]. For simplicity, we consider free pinning at the two exterior surfaces of YIG and Py and Hoffmann exchange boundary condition for the interior interface of YIG/Py [44]. From the spin wave model, we find an additional factor of $\sqrt{2}$ being multiplied to Eqs. (5b) and (5c); see the Supplemental Information for details [42]. This factor results because the nonuniform profile of the PSSW mode in YIG reduces the effective mode volume by a factor of two compared with the uniform mode. A similar effect has been previously discussed in spin pumping from PSSW modes [45, 46]. In Fig. 3(b) we plot the theoretical calculation from the spin wave model in blue dashed line, which quantitative matches to the experiments. Therefore, we conclude that the dampinglike coupling in YIG/Py bilayers are dominated by the mutual spin pumping from spin wave modes.

Fig. 4 compares the values of J and J' obtained from

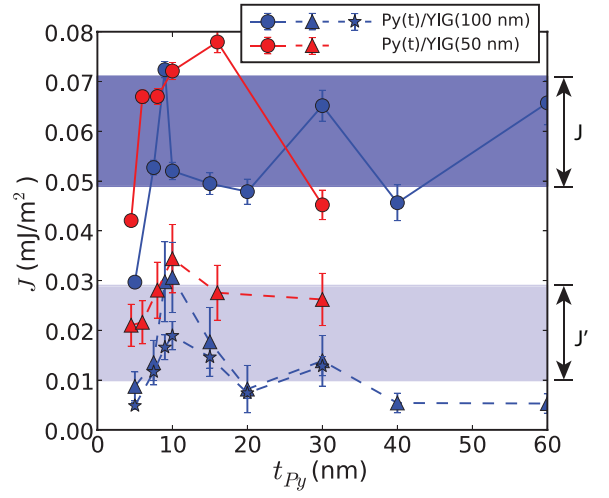


FIG. 4. Thickness dependence of J (circles) and J' (triangles), which are calculated from g_c and κ_c , respectively. Blue points denote the results for Py/YIG(100 nm) and red points for Py/YIG(50 nm). The blue stars are calculated by the linewidth enhancement between Py/YIG(100 nm) and Py. Error bars indicate single standard deviations found from the fits to the lineshape.

the hybrid dynamics. For convenience we estimate the value of J' at ω_c from Eq. (5c), as $J'(\omega_c) = \kappa_c(\omega_c)/f(\omega_c) \cdot \sqrt{M_{YIG}t_{YIG}M_{Py}t_{Py}/2}$, where $\kappa_c(\omega_c)$ is half the linewidth difference of the two hybrid modes at ω_c (Fig. 2a). We can also calculate J' from uncoupled spin pumping effect, as $J'_{sp} = \mu_0\Delta H_{sp}^{Py}(\omega_c) \cdot M_{Py}t_{Py}$. For the YIG/Py interface, the value of J stays at the same level; the value of J' fluctuates with samples but is well aligned with J'_{sp} , which again supports that the dampinglike interfacial coupling comes from spin pumping. Furthermore, we have also repeated the experiments for a thinner YIG(50 nm)/Py(t) sample series and obtained similar values of J and J' , as shown in Fig. 4.

Table I summarizes the values of J , J' and $g^{\uparrow\downarrow}$ for YIG/Py interface, where $g^{\uparrow\downarrow}$ is calculated from Eq. (4). The value of J is much smaller than a perfect exchange coupled interface, which can be estimated by $2A_{ex}/a$, with a the lattice parameter [43]. For Py, $a = 0.36$ nm and the $A_{ex}/a = 68$ mJ/m², three orders of magnitude larger than J . This suggests a considerable lattice mismatch between YIG and Py. Comparing with similar interfaces, our reported J is similar to YIG/Ni (0.03 mJ/m² [26]) and smaller than YIG/Co (0.4 mJ/m² [25]). A different interlayer exchange coupling from Ruderman-Kittel-Kasuya-Yosida interaction may generate a larger J [47–49] but a smaller $g^{\uparrow\downarrow}$ [50]. There could also be a fieldlike contribution of J from $g^{\uparrow\downarrow}$ [25, 51–54]. But since the exchange J dominates in the coupled dynamics, it is difficult to distinguish the spin mixing conductance contribution in our experiments.

The mutual spin pumping reveals an antiferromagnetic

	$J(\text{mJ/m}^2)$	$J'(\text{mJ/m}^2)$	$g^{\uparrow\downarrow} (\text{nm}^{-2})$
YIG/Py	0.060 ± 0.011	0.019 ± 0.009	42 ± 21

TABLE I. Interfacial coupling energy and spin mixing conductance for YIG/Py.

exchange coupling from the YIG/Py interface. At ω_c (Fig. 2a) the hybrid mode with a higher resonance field exhibit a broader linewidth. Because the spin pumping is dissipative, the sign of κ_c must be positive and the mode with a broader (narrower) linewidth corresponds to the out-of-phase (in-phase) precession mode. However, the out-of-phase mode exhibit a higher resonance field than the in-phase mode. This is a signature of antiferromagnetic coupling [25]. From the resonance analysis we also find that all the SiO₂/Py samples show lower resonance fields than the Py samples grown on YIG [42], which agrees with the antiferromagnetic nature of the YIG/Py interfacial coupling.

The dampinglike coupling can be used to modulate the magnon-magnon coupling coherence. For YIG(100 nm)/Py(9 nm), the total linewidths of the two hybrid modes at ω_c , which characterize the damping rates of the Rabi-like oscillation between YIG and Py, differ by a factor of 3.4 [42]. The cooperativity can be estimated as $C_{\text{hybrid}} = (2g_c/\mu_0\Delta H_{1/2}^{\text{hybrid}})^2$, which equals to 21.8 for the in-phase mode and 1.9 for the out-of-phase mode, in comparison to $C = g_c^2/\kappa_{\text{YIG}}\kappa_{\text{Py}} = 5.0$ before considering the dampinglike coupling.

In conclusion, we have characterized the dampinglike coupling torque between two exchange-coupled ferromagnetic thin films. By exciting the hybrid dynamics in the strong coupling regime, this dampinglike torque can either increase or suppress the total damping in the out-of-phase or in-phase mode, respectively. The origin of the dampinglike torque is the coherent spin pumping from the coupling magnetization dynamics. Our results reveal new insight for tuning the coherence in magnon-magnon hybrid dynamics and are important for magnon-based coherent information processing.

Work at Argonne on sample preparation was supported by the U.S. DOE, Office of Science, Materials Sciences and Engineering Division, while work at Argonne and National Institute of Standards and Technology (NIST) on data analysis and theoretical modeling was supported as part of Quantum Materials for Energy Efficient Neuro-morphic Computing, an Energy Frontier Research Center funded by the U.S. DOE, Office of Science. Work on experimental design at Oakland University was supported by AFOSR under grant no. FA9550-19-1-0254. V.A. acknowledges support under the Cooperative Research Agreement between the University of Maryland and the NIST Center for Nanoscale Science and Technology, Award No. 70NANB14H209, through the University of Maryland. Work on microwave spectroscopy at

Columbia University was supported by NSF under grant nsf-dmr1411160.

* web54@columbia.edu

† Current address: Department of Materials Science and Engineering,

‡ weizhang@oakland.edu

- [1] M. H. Devoret and R. J. Schoelkopf, *Science* **339**, 1169 (2013).
- [2] D. D. Awschalom, L. C. Bassett, A. S. Dzurak, E. L. Hu, and J. R. Petta, *Science* **339**, 1174 (2013).
- [3] F. J. Dyson, *Phys. Rev.* **102**, 1217 (1956).
- [4] A. V. Chumak, V. I. Vasyuchka, A. A. Serga, and B. Hillebrands, *Nature Physics* **11**, 453 (2015).
- [5] A. Khitun, M. Bao, and K. L. Wang, *IEEE Trans. Magn.* **44**, 2141 (2008).
- [6] T. Schneider, A. A. Serga, B. Leven, B. Hillebrands, R. L. Stamps, and M. P. Kostylev, *Appl. Phys. Lett.* **92**, 022505 (2008).
- [7] V. V. Kruglyak, S. O. Demokritov, and D. Grundler, *J Phys. D: Appl. Phys.* **43**, 264001 (2010).
- [8] S. Kaka, M. R. Pufall, W. H. Rippard, T. J. Silva, S. E. Russek, and J. A. Katine, *Nature* **437**, 389 (2005).
- [9] F. B. Mancoff, N. D. Rizzo, B. N. Engel, and S. Tehrani, *Nature* **437**, 393 (2005).
- [10] N. Locatelli, A. Hamadeh, F. Abreu Araujo, A. D. Belanovsky, P. N. Skirdkov, R. Lebrun, V. V. Naletov, K. A. Zvezdin, M. Muñoz, J. Grollier, O. Klein, V. Cros, and G. de Loubens, *Sci. Rep.* **5**, 17039 (2015).
- [11] Y. Li, X. de Milly, F. Abreu Araujo, O. Klein, V. Cros, J. Grollier, and G. de Loubens, *Phys. Rev. Lett.* **118**, 247202 (2017).
- [12] R. Lebrun, S. Tsunegi, P. Bortolotti, H. Kubota, A. S. Jenkins, M. Romera, K. Yakushiji, A. Fukushima, J. Grollier, S. Yuasa, and V. Cros, *Nat. Commun.* **8**, 15825 (2017).
- [13] A. Awad, P. Durrenfeld, A. Houshang, M. Dvornik, E. Iacocca, R. K. Dumas, and J. Åkerman, *Nature Phys.* **13**, 292 (2017).
- [14] D. Vodenicarevic, N. Locatelli, F. Abreu Araujo, J. Grollier, and D. Querlioz, *Sci. Rep.* **7**, 44772 (2017).
- [15] M. Romera, P. Talatchian, S. Tsunegi, F. Abreu Araujo, V. Cros, P. Bortolotti, J. Trastoy, K. Yakushiji, A. Fukushima, H. Kubota, S. Yuasa, M. Ernoult, D. Vodenicarevic, T. Hirtzlin, N. Locatelli, D. Querlioz, and J. Grollier, *Nature* **563**, 230 (2018).
- [16] H. Huebl, C. W. Zollitsch, J. Lotze, F. Hocke, M. Greifenstein, A. Marx, R. Gross, and S. T. B. Goennenwein, *Phys. Rev. Lett.* **111**, 127003 (2013).
- [17] Y. Tabuchi, S. Ishino, T. Ishikawa, R. Yamazaki, K. Usami, and Y. Nakamura, *Phys. Rev. Lett.* **113**, 083603 (2014).
- [18] X. Zhang, C.-L. Zou, L. Jiang, and H. X. Tang, *Phys. Rev. Lett.* **113**, 156401 (2014).
- [19] M. Goryachev, W. G. Farr, D. L. Creedon, Y. Fan, M. Kostylev, and M. E. Tobar, *Phys. Rev. Applied* **2**, 054002 (2014).
- [20] L. Bai, M. Harder, Y. P. Chen, X. Fan, J. Q. Xiao, and C.-M. Hu, *Phys. Rev. Lett.* **114**, 227201 (2015).
- [21] Y. Li, T. Polakovic, Y.-L. Wang, J. Xu, S. Lendinez, Z. Zhang, J. Ding, T. Khaire, H. Saglam,

- R. Divan, J. Pearson, W.-K. Kwok, Z. Xiao, V. Novosad, A. Hoffmann, and W. Zhang, *Phys. Rev. Lett.* **123**, 107701 (2019).
- [22] J. T. Hou and L. Liu, *Phys. Rev. Lett.* **123**, 107702 (2019).
- [23] Y. Tabuchi, S. Ishino, A. Noguchi, T. Ishikawa, R. Yamazaki, K. Usami, and Y. Nakamura, *Science* **349**, 405 (2015).
- [24] D. Lachance-Quirion, Y. Tabuchi, S. Ishino, A. Noguchi, T. Ishikawa, R. Yamazaki, and Y. Nakamura, *Science Advances* **3** (2017), 10.1126/sciadv.1603150.
- [25] S. Klingler, V. Amin, S. Geprags, K. Ganzhorn, H. Maier-Flaig, M. Althammer, H. Huebl, R. Gross, R. D. McMichael, M. D. Stiles, S. T. B. Goennenwein, and M. Weiler, *Phys. Rev. Lett.* **120**, 127201 (2018).
- [26] J. Chen, C. Liu, T. Liu, Y. Xiao, K. Xia, G. E. W. Bauer, M. Wu, and H. Yu, *Phys. Rev. Lett.* **120**, 217202 (2018).
- [27] H. Qin, S. J. Hamalainen, and S. van Dijken, *Sci. Rep.* **8**, 5755 (2018).
- [28] C. Liu, J. Chen, T. Liu, F. Heimbach, H. Yu, Y. Xiao, J. Hu, M. Liu, H. Chang, T. Stueckler, S. Tu, Y. Zhang, Y. Zhang, P. Gao, Z. Liao, D. Yu, K. Xia, N. Lei, W. Zhao, and M. Wu, *Nature Commun.* **9**, 738 (2018).
- [29] K. An, V. Bhat, M. Mruczkiewicz, C. Dubs, and D. Grundler, *Phys. Rev. Applied* **11**, 034065 (2019).
- [30] Y. Tserkovnyak, A. Brataas, and G. E. W. Bauer, *Phys. Rev. Lett.* **88**, 117601 (2002).
- [31] B. Heinrich, Y. Tserkovnyak, G. Woltersdorf, A. Brataas, R. Urban, and G. E. W. Bauer, *Phys. Rev. Lett.* **90**, 187601 (2003).
- [32] K. Lenz, T. Toliński, J. Lindner, E. Kosubek, and K. Baberschke, *Phys. Rev. B* **69**, 144422 (2004).
- [33] Y. Tserkovnyak, A. Brataas, G. E. W. Bauer, and B. I. Halperin, *Rev. Mod. Phys.* **77**, 1375 (2005).
- [34] S. S.-L. Zhang and S. Zhang, *Phys. Rev. B* **86**, 214424 (2012).
- [35] V. P. Amin, J. Zemen, and M. D. Stiles, *Phys. Rev. Lett.* **121**, 136805 (2018).
- [36] Y. S. Chen, J. G. Lin, S. Y. Huang, and C. L. Chien, *Phys. Rev. B* **99**, 220402 (2019).
- [37] B. F. Miao, S. Y. Huang, D. Qu, and C. L. Chien, *Phys. Rev. Lett.* **111**, 066602 (2013).
- [38] P. Hyde, L. Bai, D. M. J. Kumar, B. W. Southern, C.-M. Hu, S. Y. Huang, B. F. Miao, and C. L. Chien, *Phys. Rev. B* **89**, 180404 (2014).
- [39] S. Li, W. Zhang, J. Ding, J. E. Pearson, V. Novosad, and A. Hoffmann, *Nanoscale* **8**, 388 (2016).
- [40] M. B. Jungfleisch, V. Lauer, R. Neb, A. V. Chumak, and B. Hillebrands, *Appl. Phys. Lett.* **103**, 022411 (2013).
- [41] S. Klingler, A. V. Chumak, T. Mewes, B. Khodadadi, C. Mewes, C. Dubs, O. Surzhenko, B. Hillebrands, and A. Conca, *J. Phys. D: Appl. Phys.* **48**, 015001 (2014).
- [42] See the Supplemental Information for details.
- [43] B. Hillebrands, *Phys. Rev. B* **41**, 530 (1990).
- [44] F. Hoffmann, A. Stankoff, and H. Pascard, *J. Appl. Phys.* **41**, 1022 (1970).
- [45] A. Kapelrud and A. Brataas, *Phys. Rev. Lett.* **111**, 097602 (2013).
- [46] Y. Li and W. E. Bailey, *Phys. Rev. Lett.* **116**, 117602 (2016).
- [47] S. S. P. Parkin, N. More, and K. P. Roche, *Phys. Rev. Lett.* **64**, 2304 (1990).
- [48] M. Belmeguenai, T. Martin, G. Woltersdorf, M. Maier, and G. Bayreuther, *Phys. Rev. B* **76**, 104414 (2007).
- [49] L. Fallarino, V. Sluka, B. Kardasz, M. Pinarbasi, A. Berger, and A. D. Kent, *Appl. Phys. Lett.* **109**, 082401 (2016).
- [50] H. Yang, Y. Li, and W. E. Bailey, *Appl. Phys. Lett.* **108**, 242404 (2016).
- [51] W. Zhang, M. B. Jungfleisch, F. Freimuth, W. Jiang, J. Sklenar, J. E. Pearson, J. B. Ketterson, Y. Mokrousov, and A. Hoffmann, *Phys. Rev. B* **92**, 144405 (2015).
- [52] J. Sklenar, W. Zhang, M. B. Jungfleisch, W. Jiang, H. Chang, J. E. Pearson, M. Wu, J. B. Ketterson, and A. Hoffmann, *Phys. Rev. B* **92**, 174406 (2015).
- [53] T. Nan, S. Emori, C. T. Boone, X. Wang, T. M. Oxholm, J. G. Jones, B. M. Howe, G. J. Brown, and N. X. Sun, *Phys. Rev. B* **91**, 214416 (2015).
- [54] L. Zhu, D. C. Ralph, and R. A. Buhrman, *Phys. Rev. Lett.* **123**, 057203 (2019).